CONDENSED MATTER PHYSICS

Quantitative hyperspectral coherent diffractive imaging spectroscopy of a solid-state phase transition in vanadium dioxide

Allan S. Johnson[1]*, Jordi Valls Conesa[1], Luciana Vidas[1], Daniel Perez-Salinas[1], Christian M. Günther[2†], Bastian Pfau[3], Kent A. Hallman[4], Richard F. Haglund Jr.[4], Stefan Eisebitt[2,3], Simon Wall[1,5]*

Solid-state systems can host a variety of thermodynamic phases that can be controlled with magnetic fields, strain, or laser excitation. Many phases that are believed to exhibit exotic properties only exist on the nanoscale, coexisting with other phases that make them challenging to study, as measurements require both nanometer spatial resolution and spectroscopic information, which are not easily accessible with traditional x-ray spectromicroscopy techniques. Here, we use coherent diffractive imaging spectroscopy (CDIS) to acquire quantitative hyperspectral images of the prototypical quantum material vanadium oxide across the vanadium $L_{2,3}$ and oxygen K x-ray absorption edges with nanometer-scale resolution. We extract the full complex refractive indices of the monoclinic insulating and rutile conducting phases of VO_2 from a single sample and find no evidence for correlation-driven phase transitions. CDIS will enable quantitative full-field x-ray spectromicroscopy for studying phase separation in time-resolved experiments and other extreme sample environments where other methods cannot operate.

INTRODUCTION

The rich diversity of thermodynamic phases in solid-state systems results in a wide range of properties and behaviors, and the study of phase diagrams—the behavior of the system under different thermodynamic conditions—constitutes a major branch of investigation in condensed matter physics (*1*). In complex materials, many different phases can emerge through the interplay of the spin, charge, and lattice degrees of freedom, and these different phases can coexist at the nanoscale. When under extreme stimuli such as high magnetic fields and temperatures or exposed to ultrafast laser excitation, previously unidentified material phases can emerge that have unexpected and potentially useful properties; for instance, room temperature superconductivity now famously emerges at extremely high pressures (*2*). In materials showing phase coexistence, these "hidden" phases may emerge only at the nanoscale, with the presence of other phases either intrinsically competing with or even being necessary for the stability of the novel phase. These nanoscale phases have been posited to exist in a wide range of materials including prototypical systems such as the cuprates (*3*–*5*) and manganites (*6*, *7*) but are perhaps most famously proposed to exist in the vanadates. Vanadates form one of the most widely studied groups of quantum materials because of their prototypical metal-to-insulator (IMT) phase transition (*8*) and their catalytic properties (*9*, *10*).

Many experiments in the vanadates have suggested that novel correlated phases can exist in equilibrium on the nanoscale close to the IMT, which are different from those found in the bulk. For example, both V_2O_3 (*11*) and VO_2 (*12*, *13*) have been reported to exhibit correlation-driven nanoscale metallic phases the critical temperature (T_c). VO_2 in particular is also claimed to exhibit a nonequilibrium nanoscale phase after optical excitation (*14*–*16*). Many of these claims have not directly observed the phase but inferred it from combining multiple techniques. Such an approach has been shown to be unreliable, and the presence of these "hidden" phases remains unproven (*17*). Thus, understanding emergent phases in these complex and spatially inhomogeneous materials requires nanoscale imaging methods that are compatible with the extreme conditions under which they are generated and can return information on the local spin, charge, and lattice state. While electron diffraction has been shown to measure dynamical phase coexistence at the nanoscale (*18*), multiple probes are needed to determine the properties of materials. Specifically, metal-insulator transitions may not show a structural change. Another promising method is x-ray spectromicroscopy, which leverages the power of x-ray spectroscopy to provide the sensitivity to electronic, chemical, and bond-angle makeup in nanoscale systems necessary to understand nanoscale phase separation (*19*, *20*). X-ray spectroscopy is already widely used to study phase transitions because of this sensitivity (*12*, *21*–*23*), and x-ray spectromicroscopy is already used to study emergent phase coexistence at the nanoscale in some systems (*24*). However, x-ray imaging methods are limited by available x-ray optics, restricting their spatial resolution, bandwidth, and sample geometries (*19*). In particular, conventional x-ray optics need to be very close (≈1 μm) to the sample to achieve nanometer resolution, hampering the use of high magnetic fields or laser excitation. To surpass these limits, coherent scattering methods such as coherent diffractive imaging (CDI) and ptychography have been developed, which do not rely on the x-ray optics but rather on the coherence of the beam to achieve high spatial resolution (*25*, *26*). Coherent imaging methods can achieve diffraction-limited resolution while having the advantage of returning the full complex amplitude and phase of the sample. Coherent imaging methods work by numerically inverting the captured scattering pattern of the

[1]ICFO-Institut de Ciencies Fotoniques, The Barcelona Institute of Science and Technology, Barcelona, Spain. [2]Institut für Optik und Atomare Physik, Technische Universität Berlin, 10623 Berlin, Germany. [3]Max-Born-Institut, 12489 Berlin, Germany. [4]Department of Physics and Astronomy, Vanderbilt University, Nashville, TN 37235-1807, USA. [5]Department of Physics and Astronomy, Aarhus University, Ny Munkegade 120, 8000 Aarhus C, Denmark.
*Corresponding author. Email: allan.johnson@icfo.eu (A.S.J.); simon.wall@phys.au.dk (S.W.)
†Present address: Technische Universität Berlin, Zentraleinrichtung Elektronenmikroskopie (ZELMI), 10623 Berlin, Germany.

sample, and a variety of geometries are possible that are compatible both with time-resolved measurements (*27*, *28*) and with samples in complex environments (*25*, *29*). The important role that coherent scattering imaging methods could have in understanding phase transitions at the nanoscale has been previously recognized (*26*), but imaging is only part of the story. Methods that can also identify the properties of nanophases are also needed, and to date, no measurements discriminating different solid-state phases have been demonstrated.

Measuring nanoscale solid-state phases presents new challenges for coherent imaging methods. First, we note that while solid-to-solid phase transitions can modulate the density of the material, the density-length product is unchanged, and this quantity is the relevant value for imaging of two-dimensional (2D) objects. Hard x-ray coherent imaging can directly measure changes in structure and density (*26*), but many phase transitions show either no or marginal changes in structure; measuring the minor structural changes associated with some phase transitions is challenging even for large macroscopic crystals where the sensitivity is intrinsically many orders of magnitude larger than for nanoscale imaging methods (*30*). Thus, large density-related changes cannot be expected to provide a strong contrast mechanism as in other systems commonly studied with coherent imaging (*31*, *32*). As already indicated, an alternative route is to use the sensitivity of x-ray spectroscopy to changes in the local electronic and nuclear structure to determine the phase makeup. Coherent imaging has been combined with x-ray spectroscopy in the past, most notably with x-ray ptychography where spectral information has been used to measure chemical makeup and charge states (*33*–*36*), although dichroic CDI measurements mapping the presence of a particular element or magnetic domains are common as well (*37*–*39*). Dichroic measurements rely on a priori knowledge of the material properties and usually leverage a strong contrast mechanism; changes of 15% are common for magnetic dichroism, while the presence or lack thereof of an element can easily change the scattering probability by orders of magnitude when tuned to an absorption edge. Measurement of charge states (also commonly referred to as oxidization or valency states) on the other hand is conceptually very similar to the measurement of phases, as in both cases the different states manifest as changes in the x-ray absorption spectrum (XAS) due to local alterations of the electronic structure. However, discriminating and identifying phases can be more challenging than charge states; charge states are identifiable through the chemical shift of the absorption edge and exhibit other large changes in the XAS, while phase transitions can result in much more subtle changes distributed across the full absorption spectrum. Particularly for phases that emerge only at the nanoscale, the ability to perform truly quantitative measurements of the XAS becomes critically important, as each portion of the spectrum reports on different aspects of the material properties.

Here, we present the first quantitative x-ray spectromicroscopy of solid-state phases using coherent imaging. We extend CDI to a full spectromicroscopy method, CDI spectroscopy (CDIS), capable of returning the full spectroscopic and nanometer-scale spatial information from a variety of samples. In a geometry compatible with ultrafast laser excitation and high magnetic fields, we acquire hyperspectral images of a vanadium oxide thin film with 25-nm spatial and 0.25-eV spectral resolution across the vanadium $L_{2,3}$ and oxygen K-edges. We note a previously unappreciated ambiguity of coherent imaging methods in the determination of the sample plane that leads to distortions of the extracted XAS spectrum and outline a procedure for finding the correct object plane, allowing us to recover the complex refractive index of the sample. We show that our sample is a heterogeneous mixture of approximately 80% VO_2 and 20% V_2O_5 using this data. We then heat the sample to observe the phase transition from the monoclinic insulating (M) to rutile conducting (R) phase in the VO_2 and extract the full amplitude and phase for all three different states simultaneously. We see no evidence of any intermediate phases, either insulating or metallic, and show that a previously observed intermediate phase we measured with x-ray holography resulted from the ambiguity in object plane. Our results pave the way for the quantitative study of novel nanoscale solid-state phases in a wide range of cases inaccessible to current x-ray spectromicroscopy methods.

RESULTS

Quantitative CDIS

A 75-nm-thick film of nominally vanadium oxide, masked to provide the finite spatial extent needed for numerical inversion, was illuminated with synchrotron radiation and the resulting diffraction pattern recorded on a charge-coupled device (CCD) detector (Fig. 1). The nearest beamline optic to the system is several meters away; hence, the method is compatible with laser excitation and strong magnetic fields, along with other environments. The required target stability is low, allowing us to heat the sample without the need for any active stabilization. Reference holes in the mask provide an absolute phase reference for the input wave, allowing us to quantitatively extract both components of the complex refractive index $n = 1 - \delta - i\beta$ and not just the relative phase shift between different parts of the sample. While these references also permit a Fourier transform holography (FTH) analysis of the sample (*40*), substantial low-frequency noise in the reconstruction prevents quantitative spectroscopy (section S1 and fig. S1), and a full CDI analysis is found to be necessary.

Although there has been an increasing push for coherent imaging methods that can operate with broadband illumination, spectral scanning of the x-ray wavelength is still required for identification of solid phases from their absorption spectra. In particular, recent broadband CDI measurements require negligible spectral structure in the sample (*41*), while proposed hybrid scanning-CDI methods return only coarse spectral structure (*42*); thus, neither can return the XAS spectrum required for phase identification. In our approach, no chromatic elements are used, allowing us to scan the x-ray photon energy from 510 to 535 eV without any adjustments in the optical layout between images, and 101 images were taken in 0.25-eV steps of photon energy. Further details on the sample and experimental methods are given in Materials and Methods.

We invert the diffraction patterns at each photon energy independently to generate real-space images using an iterative phase reconstruction algorithm robust to partial coherence (see Materials and Methods). Concatenating these images leads to a hyperspectral image where each pixel contains the full amplitude and phase of the local XAS spectrum or the local complex refractive index. Extraction of quantitative spectral information from coherent imaging methods is, however, complicated by the fact that coherent imaging methods return a complex real-space image, which can be numerically propagated to other planes. This propagation is necessary as the initial image will be at a particular plane in space, which may or may not

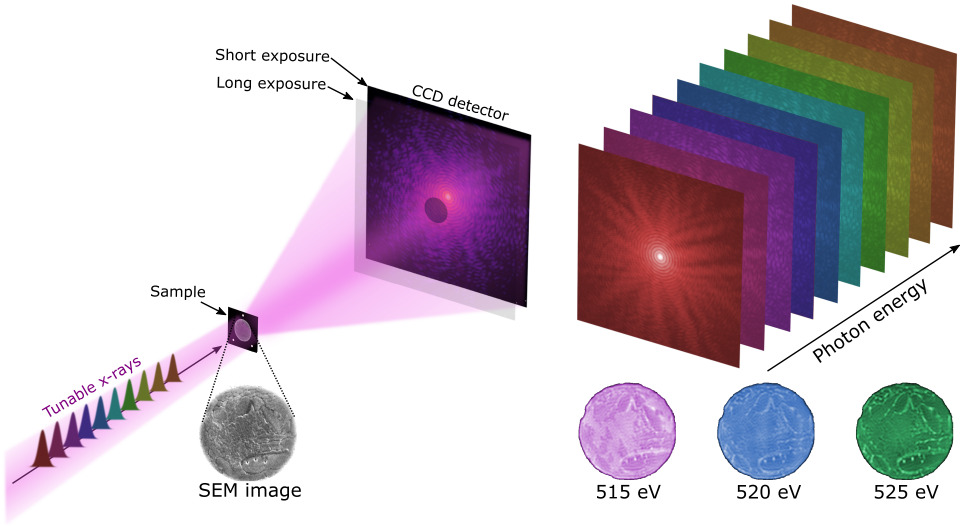

Fig. 1. Experimental setup for CDIS. A tunable synchrotron x-ray radiation source illuminates the sample, and the scattered radiation is collected on a CCD camera. Holographic reference holes in the sample mask provide an absolute phase reference. Long and short exposures are combined to yield a high dynamic range diffraction pattern. Images are recorded at a range of photon energies across the relevant absorption edges; three representative amplitude images are shown.

correspond to the actual object plane. For instance, in holography, this is the plane of the mask, while in CDI, it is set by the applied spatial constraint: the plane of the aperture in a sample with a mask or the plane of the smallest spatial size for an isolated object (*43*). Away from the correct plane, the propagation leads to coupling between the amplitude and phase channels, as described by the mathematics of optical or contrast transfer functions (*44*, *45*). This amplitude-phase coupling is perhaps most famously illustrated in the use of propagation to generate shadow images of phase-only objects (*46*). To extract quantitative information such as the δ and β of the sample in a 2D geometry, it is thus critical to analyze features in the object plane.

The sample plane is most often selected by choosing a feature and propagating until it is in focus, which is to say when it forms the sharpest image. In noncoherent methods, this procedure is generally well defined, but in coherent imaging methods, there is an inherent ambiguity in choosing whether to bring the amplitude or phase component into focus. For instance, an amplitude-only object that was propagated until the phase component came into focus would map to the wrong plane and create an apparent but artificial phase component to the sample, as shown in Fig. 2; the inverse relationship also holds. If only one contrast mechanism (amplitude or phase) is consequential and is known a priori, then the propagation is performed to bring the correct component into focus. Alternatively, and more generally, the artificial propagation–induced amplitude or phase components flip sign as they are propagated through the object plane, while the real components maintain their physically meaningful sign. This can be seen from a Huygens principle view of a source plane, where each point acts a source of a spherical wavelet; propagation through the object plane converts each outgoing spherical wave into an incoming one, inverting the sign. These principles allow us to identify the correct sample plane and extract quantitative information. We have combined both approaches here. Since a normal Lorentzian absorption peak introduces no phase shift at the peak of the absorption, we propagate until the amplitude component came into focus at photon energies corresponding to peaks of the absorption spectrum, where the contrast is dominantly in the amplitude channel, and verifying that the phase flipped sign around this point. The propagation required is the same for all wavelengths as the iterative reconstruction algorithms reconstruct all wavelengths at the constraint (mask) plane. How widespread this issue is in previous measurements is unclear as physically plausible images are returned away from this plane, but it appears to not have been noted previously.

Having identified the correct object plane, we use the hyperspectral image to generate false-color images where the different red-green-blue color channels encode a variety of spectral bands. Figure 3A shows a comparison between a scanning electron microscopy (SEM) micrograph and a false-color amplitude image of the sample at 320 K that we composed from eight different frequency bands chosen to highlight all states of interest while remaining visible to those with color blindness (see Materials and Methods). A comparison of the finest features observed in the CDIS reveals a resolution of 25 nm in the maximum q direction (fig. S6). Thickness changes, reflecting the topography of the sample, are apparent in all individual images and as blue-white features in the composite image, agreeing very well with the SEM micrograph. Most notably, however, we can see two major regions of the sample (pink and green) that are not apparent from the SEM image. To identify these regions, we extract the local x-ray absorption spectra from the hyperspectral image, which are plotted in Fig. 3B, along with the integrated spectrum of the whole sample. Clear differences appear particularly on the vanadium $L_{2,3}$-edges (≈518 and ≈522 eV). The assignment of features in the XAS spectra of vanadium oxides is well established (*22*, *47*–*50*), which allow us to identify the pink regions as monoclinic insulating phase (M1) VO_2 and the green region as V_2O_5. In particular, the absorption peak at 516 eV and the resonance at 522 eV are much more pronounced in VO_2, while the ratio of the two oxygen peaks at 529 and 532 eV also acts as a marker for the charge state (*22*, *50*). Furthermore, while forward scattering CDI is generally insensitive to the crystal orientation when off-resonance, the XAS spectra of anisotropic materials are themselves strongly anisotropic,

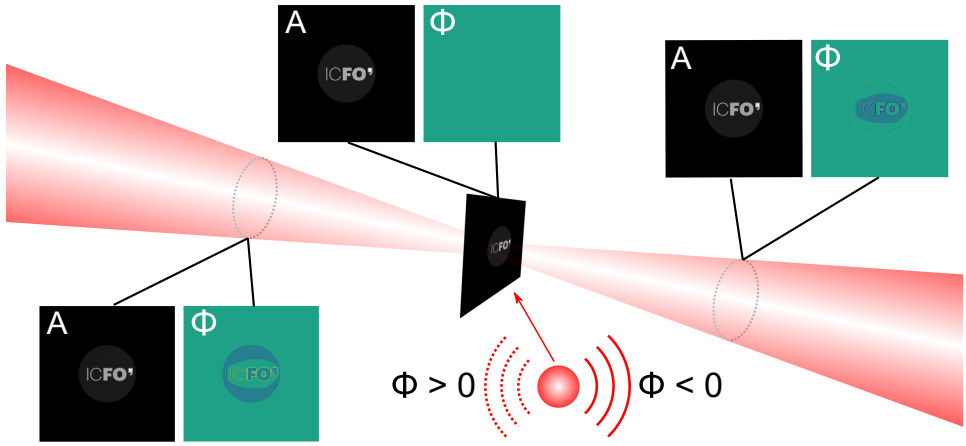

Fig. 2. Effect on propagation of an originally purely amplitude image. Amplitude (A) and phase (Φ) of an amplitude-only object imaged before, at, and after the object plane. Propagation causes features in the amplitude channel to appear in the phase channel. The artificial propagation–induced phase changes sign through the real focus at the object plane.

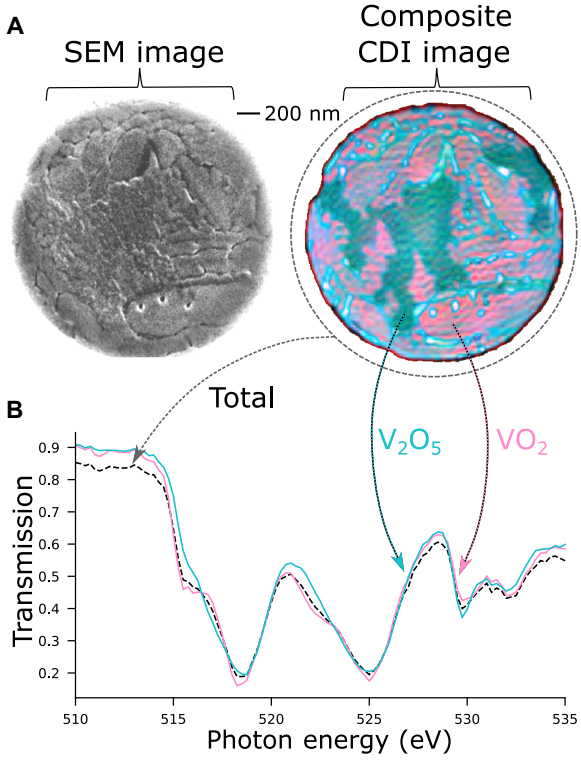

Fig. 3. Hyperspectral imaging of a vanadium thin film. (**A**) SEM image of the sample and comparison to a false-color composite image of the sample at 320 K. Scale bar, 200 nm. Two different regions (pink and green) are clearly visible in addition to the topography (blue-white). The composite is formed from a combination of images taken at individual photon images. A total of 101 monochromatic images are taken, allowing us to extract a full transmission spectrum for each pixel in a hyperspectral imaging scheme. Comparison of lineouts around the finest spatial features reveals a spatial resolution of 25 nm. (**B**) Transmission spectra of the pink and green regions of the sample, along with the integrated spectrum as would be observed in absorption spectroscopy (black). The full spectral information allows us to identify the green region as V_2O_5 and the pink as monoclinic phase VO_2.

and clear differences depending on the crystal orientation relative to the x-ray polarization can be found. In M1-phase VO_2 (*51*), shifts of around 1 eV would be expected in the peak at 516 eV and the resonance at 522 eV for perpendicularly orientated samples, but such large features are absent, and a homogenous spectrum is observed across all VO_2 regions. In V_2O_5, the orientation manifests as the appearance or lack thereof of additional peaks between 516 and 520 eV changes in the relative peak heights at the oxygen edge (*52*); no such changes are observed in the sample. Thus, we conclude that the crystallites in this field of view have the same orientation of their anisotropy axis.

Despite V_2O_5 making up 20% of the sample and the large differences in their spectra, the integrated spectrum is broadly consistent with that of the nominal film composition, VO_2, underlining the necessity of spectroscopic imaging methods in accurately determining local material composition. We note that in the pre-edge spectrum, the overall transmission is lower than for either the VO_2 or V_2O_3; this is due to defects in the sample that absorb more strongly off-resonance than the vanadate portion but on resonance become less important. Our results, which show a substantial V_2O_5 fraction, may be of interest for the manufacturing of VO_2-based devices as the thin films were deposited using the commonly used technique of pulsed laser deposition (PLD) and subsequent annealing (*53*), although previous work has shown that some V_2O_5 in PLD films does not adversely affect the switching behavior of the entire film (*54*). The boundary between the V_2O_5 and VO_2 regions does not always correspond to a distinct topographic feature in the SEM or off-resonant CDI images, demonstrating the ability of CDIS to track oxygen diffusion that is not visible to nonspectroscopic imaging.

Complex spectromicroscopy of an insulator-to-metal phase transition

We next use the coherent nature of CDIS together with our reference structure to examine the IMT phase transition of VO_2 and extract the complex refractive index of each phase. As we heat the sample through the VO_2 phase transition (≈336 K), regions of the rutile metallic phase (R phase) begin to nucleate near crystallite edges and other defects, eventually growing to encompass the entire VO_2

volume (fig. S2) (*55*). Although the (M1) start and end (R) points of this phase transition are well known, numerous studies have speculated the existence of nanoscale intermediate phases, but no direct visualizations of these states have been possible. Therefore, we perform CDIS across the phase transition region to investigate the role of hidden phases. Figure 4A shows a false-color amplitude image of the sample when heated to 336 K, at the center of the transition. Purple regions have grown to encompass roughly 50% of the VO_2. We can see an identical structure in the phase, as seen in Fig. 4B, where an alternative set of photon energies is used to generate the false-color image (Materials and Methods). This alternative set is necessary because the phase shift imparted by an absorption resonance changes sign passing through the peak of the absorption, leading to a minimal phase shift imparted at the maximum absorption and zero contrast in phase coinciding with maximum contrast in the amplitude.

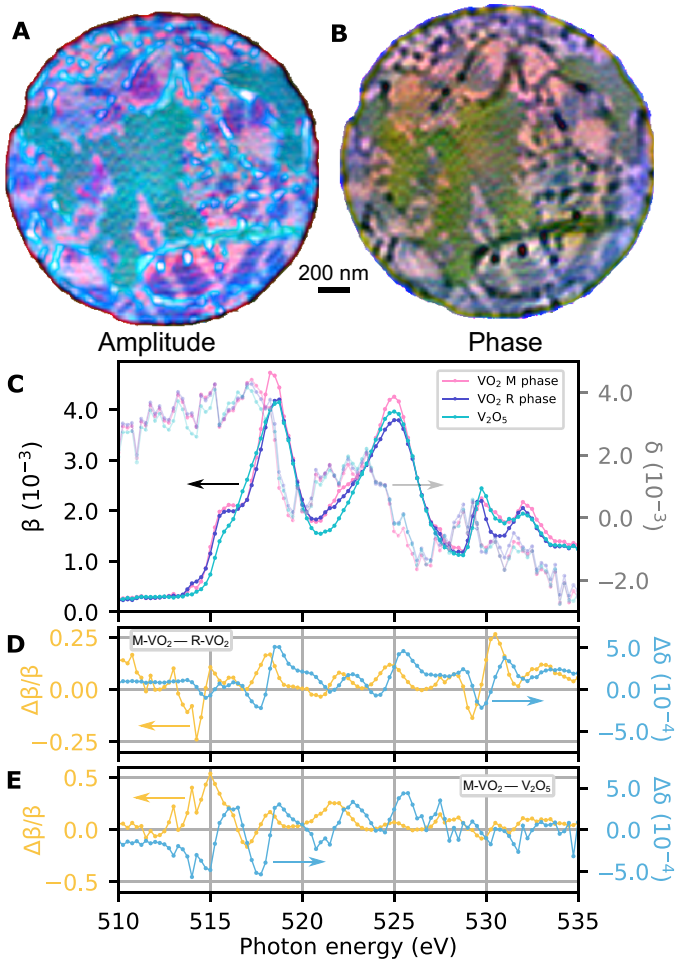

Fig. 4. Fully quantitative amplitude and phase imaging of thermodynamic phase and oxidization state coexistence in vanadium oxide. (**A**) False-color amplitude of the VO_2/V_2O_5 sample at 336 K. The new purple regions correspond to the R phase of VO_2. Scale bar, 200 nm. (**B**) Corresponding phase image. (**C**) Extracted real (solid lines) and imaginary (faded lines) parts of the refractive index for V_2O_5 and the monoclinic and rutile phases of VO_2, with colors corresponding to the false-color amplitude image. (**D**) Difference between the real and imaginary parts of the refractive index for VO_2 R and M1 phase. (**E**) Difference between the real and imaginary parts of the refractive index for V_2O_5 and VO_2 M1 phase. The standard error of the spectra calculated across their respective regions of interest results in error bars too small to be seen here.

These newly grown phase domains are readily identifiable as the R phase by comparing our data to absorption spectra found in the literature; in particular, the R phase results in a large shift in the 529-eV resonance at the oxygen edge. As a function of temperature, we only observe an increase in the metallic phase volume fraction and find no evidence for any intermediate structures, indicating direct transitions from the M1 to R phase. Our results, which show identical domains in both the amplitude and phase channels, also rule out the presence of strong strain fields that could induce a secondary transition (*56*) and show conclusively that nanoscale monoclinic metallic domains do not form during the transition.

This demonstrates the power of CDIS over conventional FTH analysis, which uses a beam block to suppress the direct beam for phase identification. Our previous FTH measurements suggested that the M2 phase formed in specific locations, which we attributed to strain. However, x-ray absorption spectra could not be obtained to confirm the M2 phase assignment. This now appears to not be the case. While the beam stop used in FTH can increase the dynamic range by suppressing the central part of the hologram, it results in mixing the real and imaginary components of the scattered field, making quantitative spectroscopy impossible and prevents the correct assignment of the object plane unless the properties of the object are already known. Amplitude-to-phase coupling via propagation of coherent x-rays then leads to the appearance of artificial phase domains (see section S3); this artifact underlies the importance of precise determination of the object plane for quantitative measurement in coherent x-ray spectromicroscopy.

Using the full complex field, we can locally extract the complex refractive index of all three constituents (V_2O_5 and R-phase and M-phase VO_2) from a single hyperspectral dataset as shown in Fig. 4C. The imaginary part of the refractive index β is in excellent agreement with previous absorption measurements for all three constituents, while the previously unmeasured real part δ provides a new constraint for ab initio models of vanadium oxides (*57*). The retrieved δ is noisier than β because the phase shift is measured relative to the reference holes, which have low amplitude because of their small size and are imaged as near single-pixel size. However, as the values at different regions are measured simultaneously and relative to the same reference, this noise cancels when considering the differences in δ and β. This also ensures that the differences are robust with respect to drift during measurement, an advantage of full-field imaging like CDI over scanning methods like ptychography. This advantage was previously noted in conventional x-ray spectromicroscopy (*58*) but in such systems applied only for absorption or phase independently. The differences in δ and β between different constituents are shown in Fig. 4 (D and E) and show oscillations characteristic of the resonance structure, with *n* and *k* oscillating out of phase. This is consistent with the Kramers-Kronig relation of the resonances and is a very effective way of identifying the exact energies of overlapping resonances. While no intermediate phases were observed in our dataset, in contrast to reports elsewhere (*12*, *55*), in the event that phases without a macroscopic counterpart were observed, such a difference analysis would allow the parent phase to act as a local reference for both amplitude and phase of the nanoscale state. This differential analysis would allow very subtle changes in the XAS to be observed. This is particularly important for detecting

domains that are below the resolution limit. For example, experiments have suggested that transient domains, of an order of 10 to 20 nm in size, may exist in VO_2 (*15*). While such domains could not be observed directly in the current approach, phase coexistence will still affect the optical properties, with reduced magnitude, on a scale that can be observed. Thus, subresolution domains with dimensions close to the resolution limit could still be inferred.

DISCUSSION

We have performed the first quantitative measurements of solid-state phases using coherent x-ray imaging by extending CDI to a full x-ray spectromicroscopy method, CDIS, demonstrating the first full-field coherent imaging spectromicroscopy method. By generating hyperspectral images of a vanadium oxide thin film spanning 510 to 535 eV and identifying the correct object plane, we recover the full complex amplitude and phase across the XAS and uniquely identify different oxidization states and phases at temperatures across the VO_2 insulator-to-metal phase transition. We return the first quantitative measurement of the complex refractive indices for V_2O_5 and the M1 and R phases of VO_2. We also rule out the presence of intermediate phases in the IMT for our sample and show that an intermediate phase previously observed with FTH is a propagation artifact, underlining the extra care that is needed for extracting even qualitative information from coherent imaging methods.

In comparison with conventional methods, we require no high–numerical aperture diffractive optics (*33*, *58*). Hence, CDIS is fully compatible with time-resolved measurements and with a wide range of sample environments, including high magnetic field and cryogenic samples, paving the way for multidimensional spectroscopic imaging of solid-state phase transitions with x-ray probes. In comparison to ptychography, CDIS requires no stabilization of the sample position, which may be prohibitive for high magnetic field geometries, and no scanning of the probe beam or sample, which is advantageous for multidimensional measurements. In addition, as CDIS is a full-field measurement, it has reduced sensitivity to drift in the x-ray source, which may be important for experiments at x-ray–free electron lasers or with high-harmonic sources.

While here a mask chosen to allow comparison of FTH and CDI was used to examine the optimal route for coherent x-ray spectromicroscopy, in the future, larger reference holes placed closer to the sample aperture can speed acquisition, reduce noise in the real part of refractive index, and relax requirements on the beam coherence without reduction in the reconstruction quality or resolution (*59*). Although the current measurements were made with 0.25-eV spectral resolution and 25-nm spatial resolution, state-of-the-art beamlines allow for sub–10-meV spectral resolution if required, while the spatial resolution is set by the scattering geometry and is ultimately diffraction limited. The spectral resolution used here, which allows for clear discrimination between material phases, corresponds to ≈15-fs transform-limited pulses, which could allow for time-resolved studies of phase transition beyond magnetic dynamics at x-ray–free electron lasers (XFELs) (*60*) or with high-harmonic generation sources (*61*). However, the slow recovery time of optically excited samples may favor the use of XFELs, which generally operate at reduced repetition rates and provide sufficient time for sample recovery (*55*, *62*). We note that moving between absorption edges separated by hundreds of electron volts, relevant for many materials, would require no changes to the setup.

Here, we have considered soft x-rays, but hard x-ray XAS can also reveal local chemical and phase changes (*63*). CDIS in the hard x-ray could be used for phase-sensitive measurements in an even greater range of sample environments, particularly at the extreme pressures in diamond anvil cells where a range of exotic phases are produced. As the wealth of material phases that emerge at the nanoscale under extreme stimuli continue to be unveiled, the ability of coherent x-ray spectromicroscopy to reveal the quantitative nature of these phases will make it an increasingly valuable tool for condensed matter physics.

MATERIALS AND METHODS

Sample preparation and data acquisition

A 75-nm-thick layer of VO_2 was deposited on a Si_3N_4 membrane using PLD and subsequent annealing (*55*). The opposite surface was coated with a $[Cr(5\ nm)/Au(55\ nm)]_{20}$ multilayer (~1.1 μm integrated Au thickness) to block the x-rays. Using a focused ion beam (FIB), a 2-μm-diameter aperture was cut in the Cr/Au multilayer to define the field of view. Three 50- to 90-nm-diameter reference apertures were FIB-milled through all three layers on a 4.5-μm radius around the central aperture.

The experiments were performed at the ALICE x-ray scattering instrument at the UE52-SGM beamline of the BESSY II synchrotron-radiation source. The sample was heated to between 300 and 360 K with 0.1 K stability. Linearly polarized x-rays were focused using a long–focal length Kirkpatrick-Baez–like mirror pair, giving a large focal spot (≈60 × 120 μm full width at half maximum) approximately 25 cm upstream from the sample itself. Diffraction patterns were acquired with a 2048 × 2048, 13.5-μm pixel x-ray CCD (Princeton Instruments MTE 2048B) placed 40 cm downstream of the sample. The maximum q direction supports a resolution of 25 nm. Ten long (3.5 to 4 s) and short (0.03 s) exposures were combined to maximize the signal to noise at the low- and high-amplitude regions before reconstruction, with a central beamblock added for the long exposures to avoid camera damage and CCD bleed. The long-exposure images were scaled to ensure that the integral over the first airy disk ring was the same between both images and combined using a circular mask with Gaussian edges.

Image reconstruction

The reference holes used to provide an absolute phase reference additionally pin the zeros of the interference fringes, improving reconstruction robustness (*38*, *59*, *64*) but at the cost of increasing the sample size to near typical transverse coherence length of third-generation synchrotrons (*65*). This necessitates the use of partial coherence reconstruction algorithms, which return both the complex object and the x-ray coherence function. Hence, reconstructions were performed using the partially coherent reconstruction algorithm of Clark *et al.* (*66*); 50 iterations of the error reduction algorithm were followed by 100 iterations of the hybrid input-output algorithm (*67*), ending with another 49 iterations of error reduction. Every 15 iterations, the coherence function was updated by 25 iterations of the Lucy-Richardson deconvolution algorithm (*68*, *69*). The use of partially coherent methods was essential to obtain good reconstructions; fully coherent methods introduced substantial low-frequency noise to the reconstruction. We found no evidence of underdetermination for the partial coherent reconstruction of complex objects as described in previous works (*64*), likely because the reference

holes, while only partially coherent, lead to sufficiently clear interference fringes to pin the reconstructed phase. Most critical to obtaining high-quality reconstructions was the accurate determination of the mask function, particularly for the hybrid input-output method; a single pixel error in the mask radius introduced substantial reconstruction noise. With correct determination of the mask, the algorithms were found to converge to the same value regardless of the initial guess. Images were reconstructed at 101 different energies and four different temperatures. By setting the pre-edge transmission to coincide with the atomic scattering factor transmission for a film of 75 nm thickness (90%), we convert the relative transmission values to absolute values. As small drifts in the synchrotron mode over time can adversely affect the spectrum, we used the nominally temperature-independent spectrum of the V_2O_5 to normalize out these effects. Example images at select photon energies, details on the object constrain, and resolution determination can be found in section S4.

False-color images

False-color images are generated to show contrast for particular phases of VO_2, using the different spectral response of the different phases in the real and imaginary part of the refractive index. To that end, the sum and difference images at various photon energies are considered to take advantage of the full spectral information. For amplitude images, the red channel was taken as the sum of images at 514.25 and 517 eV with images at 518.25 and 515.25 eV subtracted, the green channel images at 521 and 529.5 eV added with 530.5 eV subtracted, and the blue channel at 517 eV. A DC level of 0.5 was added to the red channel, and the channels were scaled by 1.6, 1, and 1.3, respectively, for plotting. Phase images were composed with the red channel taken as the sum of images at 514.75, 517.75, and 529.75 eV with images at 518.75, 522.75, and 531 eV subtracted; the green channel images at 521.5, 524, 525.5, and 528.75 eV added; and the blue channel the sum of 515 and 517.75 eV with 516.5 eV subtracted. A DC level of 0.5 was subtracted from the red channel, and the channels were scaled by 1, −1, and −1.2, respectively, for plotting. This scheme was chosen instead of a simple mapping of differences between the relative phases to different color channels for three reasons: one, to map different phases to different colors in such a way that the three phases are apparent to viewers with all major types of color blindness; two, to maximize the spectral information used to differentiate different phases, reducing the impact of reconstruction noise or sample contamination, particularly at the oxygen *K*-edge; and three, to enable the simultaneous viewing of the sample topography and phase/oxidization state separation, to better understand the relationship or lack thereof between topography and said separation.

SUPPLEMENTARY MATERIALS

Supplementary material for this article is available at http://advances.sciencemag.org/cgi/content/full/7/33/eabf1386/DC1

REFERENCES AND NOTES

1. B. Keimer, J. E. Moore, The physics of quantum materials. *Nat. Phys.* **13**, 1045–1055 (2017).
2. A. P. Drozdov, P. P. Kong, V. S. Minkov, S. P. Besedin, M. A. Kuzovnikov, S. Mozaffari, L. Balicas, F. F. Balakirev, D. E. Graf, V. B. Prakapenka, E. Greenberg, D. A. Knyazev, M. Tkacz, M. I. Eremets, Superconductivity at 250 K in lanthanum hydride under high pressures. *Nature* **569**, 528–531 (2019).
3. K. A. Cremin, J. Zhang, C. C. Homes, G. D. Gu, Z. Sun, M. M. Fogler, A. J. Millis, D. N. Basov, R. D. Averitt, Photoenhanced metastable c-axis electrodynamics in stripe-ordered cuprate $La_{1.885}Ba_{0.115}CuO_4$. *Proc. Natl. Acad. Sci. U.S.A.* **116**, 19875–19879 (2019).
4. S. Rajasekaran, J. Okamoto, L. Mathey, M. Fechner, V. Thampy, G. D. Gu, A. Cavalleri, Probing optically silent superfluid stripes in cuprates. *Science* **359**, 575–579 (2018).
5. G. Yu, C. H. Lee, A. J. Heeger, N. Herron, E. M. McCarron, Transient photoinduced conductivity in single crystals of $YBa_2Cu_3O_{6.3}$: Photodoping to the metallic state. *Phys. Rev. Lett.* **67**, 2581–2584 (1991).
6. D. Polli, M. Rini, S. Wall, R. W. Schoenlein, Y. Tomioka, Y. Tokura, G. Cerullo, A. Cavalleri, Coherent orbital waves in the photo-induced insulator-metal dynamics of a magnetoresistive manganite. *Nat. Mater.* **6**, 643–647 (2007).
7. K. Miyano, T. Tanaka, Y. Tomioka, Y. Tokura, Photoinduced insulator-to-metal transition in a perovskite manganite. *Phys. Rev. Lett.* **78**, 4257–4260 (1997).
8. Z. Shao, X. Cao, H. Luo, P. Jin, Recent progress in the phase-transition mechanism and modulation of vanadium dioxide materials. *NPG Asia Mater.* **10**, 581–605 (2018).
9. K. I. Otake, Y. Cui, C. T. Buru, Z. Li, J. T. Hupp, O. K. Farha, Single-atom-based vanadium oxide catalysts supported on metal-organic frameworks: Selective alcohol oxidation and structure-activity relationship. *J. Am. Chem. Soc.* **140**, 8652–8656 (2018).
10. M. Ek, Q. M. Ramasse, L. Arnarson, P. G. Moses, S. Helveg, Visualizing atomic-scale redox dynamics in vanadium oxide-based catalysts. *Nat. Commun.* **8**, 305 (2017).
11. A. S. McLeod, E. Van Heumen, J. G. Ramirez, S. Wang, T. Saerbeck, S. Guenon, M. Goldflam, L. Anderegg, P. Kelly, A. Mueller, M. K. Liu, I. K. Schuller, D. N. Basov, Nanotextured phase coexistence in the correlated insulator V_2O_3. *Nat. Phys.* **13**, 80–86 (2017).
12. A. X. Gray, J. Jeong, N. P. Aetukuri, P. Granitzka, Z. Chen, R. Kukreja, D. Higley, T. Chase, A. H. Reid, H. Ohldag, M. A. Marcus, A. Scholl, A. T. Young, A. Doran, C. A. Jenkins, P. Shafer, E. Arenholz, M. G. Samant, S. S. P. Parkin, H. A. Dürr, Correlation-driven insulator-metal transition in near-ideal vanadium dioxide films. *Phys. Rev. Lett.* **116**, 116403 (2016).
13. J. Laverock, S. Kittiwatanakul, A. Zakharov, Y. Niu, B. Chen, S. A. Wolf, J. W. Lu, K. E. Smith, Direct observation of decoupled structural and electronic transitions and an ambient pressure monocliniclike metallic phase of VO_2. *Phys. Rev. Lett.* **113**, 216402 (2014).
14. M. R. Otto, L. P. René de Cotret, D. A. Valverde-Chavez, K. L. Tiwari, N. Émond, M. Chaker, D. G. Cooke, B. J. Siwick, How optical excitation controls the structure and properties of vanadium dioxide. *Proc. Natl. Acad. Sci. U.S.A.* **116**, 450–455 (2019).
15. A. Sood, X. Shen, Y. Shi, S. Kumar, S. J. Park, M. Zajac, Y. Sun, L. Q. Chen, S. Ramanathan, X. Wang, W. C. Chueh, A. M. Lindenberg, Universal phase dynamics in VO_2 switches revealed by ultrafast operando diffraction. *arXiv* 2102.06013, (2021).
16. V. R. Morrison, R. P. Chatelain, K. L. Tiwari, A. Hendaoui, A. Bruhács, M. Chaker, B. J. Siwick, A photoinduced metal-like phase of monoclinic VO_2 revealed by ultrafast electron diffraction. *Science* **346**, 445–448 (2014).
17. L. Vidas, D. Schick, E. Martínez, D. Perez-Salinas, A. Ramos-Álvarez, S. Cichy, S. Batlle-Porro, A. S. Johnson, K. A. Hallman, R. F. Haglund, S. Wall, Does VO_2 host a transient monoclinic metallic phase? *Phys. Rev. X* **10**, 031047 (2020).
18. T. Danz, T. Domröse, C. Ropers, Ultrafast nanoimaging of the order parameter in a structural phase transition. *Science* **371**, 371–374 (2021).
19. A. E. Goode, A. E. Porter, M. P. Ryan, D. W. McComb, Correlative electron and x-ray microscopy: Probing chemistry and bonding with high spatial resolution. *Nanoscale* **7**, 1534–1548 (2015).
20. A. Sakdinawat, D. Attwood, Nanoscale x-ray imaging. *Nat. Photonics* **4**, 840–848 (2010).
21. D. Ruzmetov, S. D. Senanayake, S. Ramanathan, X-ray absorption spectroscopy of vanadium dioxide thin films across the phase-transition boundary. *Phys. Rev. B* **75**, 195102 (2007).
22. M. Abbate, H. Pen, M. T. Czyzyk, F. M. F. de Groot, J. C. Fuggle, Y. J. Ma, C. T. Chen, F. Sette, A. Fujimori, Y. Ueda, K. Kosuge, Soft x-ray absorption spectroscopy of vanadium oxides. *J. Electron Spectros. Relat. Phenomena* **62**, 185–195 (1993).
23. J.-H. Park, L. H. Tjeng, A. Tanaka, J. W. Allen, C. T. Chen, P. Metcalf, J. M. Honig, F. M. F. de Groot, G. A. Sawatzky, Spin and orbital occupation and phase transitions in V_2O_3. *Phys. Rev. B* **61**, 11506–11509 (2000).
24. A. Ronchi, P. Homm, M. Menghini, P. Franceschini, F. Maccherozzi, F. Banfi, G. Ferrini, F. Cilento, F. Parmigiani, S. S. Dhesi, M. Fabrizio, J.-P. Locquet, C. Giannetti, Early-stage dynamics of metallic droplets embedded in the nanotextured Mott insulating phase of V_2O_3. *Phys. Rev. B* **100**, 075111 (2019).
25. H. N. Chapman, K. A. Nugent, Coherent lensless x-ray imaging. *Nat. Photonics* **4**, 833–839 (2010).
26. J. Miao, T. Ishikawa, I. K. Robinson, M. M. Murnane, Beyond crystallography: Diffractive imaging using coherent x-ray light sources. *Science* **348**, 530–535 (2015).
27. J. N. Clark, L. Beitra, G. Xiong, A. Higginbotham, D. M. Fritz, H. T. Lemke, D. Zhu, M. Chollet, G. J. Williams, M. Messerschmidt, B. Abbey, R. J. Harder, A. M. Korsunsky, J. S. Wark, I. K. Robinson, Ultrafast three-dimensional imaging of lattice dynamics in individual gold nanocrystals. *Science* **341**, 56–59 (2013).
28. T. A. Assefa, Y. Cao, S. Banerjee, S. Kim, D. Kim, H. Lee, S. Kim, J. H. Lee, S. Y. Park, I. Eom, J. Park, D. Nam, S. Kim, S. H. Chun, H. Hyun, K. sook Kim, P. Juhas, E. S. Bozin, M. Lu, C. Song, H. Kim, S. J. L. Billinge, I. K. Robinson, Ultrafast x-ray diffraction study of melt-front dynamics in polycrystalline thin films. *Sci. Adv.* **6**, eaax2445 (2020).
29. J. Vura-Weis, C. Jiang, C. Liu, H. Gao, J. M. Lucas, F. M. F. de Groot, P. Yang, A. P. Alivisatos, S. R. Leone, Femtosecond $M_{2,3}$-edge spectroscopy of transition-metal oxides: Photoinduced oxidation state change in α-Fe_2O_3. *J. Phys. Chem. Lett.* **4**, 3667–3671 (2013).

30. J. Herrero-Martín, J. Blasco, J. García, G. Subías, C. Mazzoli, Structural changes at the semiconductor-insulator phase transition in the single-layered perovskite $La_{0.5}Sr_{1.5}MnO_4$. *Phys. Rev. B.* **83**, 184101 (2011).
31. L.-M. Stadler, C. Gutt, T. Autenrieth, O. Leupold, S. Rehbein, Y. Chushkin, G. Grübel, Hard x ray holographic diffraction imaging. *Phys. Rev. Lett.* **100**, 245503 (2008).
32. K. A. Nugent, T. E. Gureyev, D. F. Cookson, D. Paganin, Z. Barnea, Quantitative phase imaging using hard x rays. *Phys. Rev. Lett.* **77**, 2961–2964 (1996).
33. D. A. Shapiro, Y.-S. Yu, T. Tyliszczak, J. Cabana, R. Celestre, W. Chao, K. Kaznatcheev, A. L. D. Kilcoyne, F. Maia, S. Marchesini, Y. S. Meng, T. Warwick, L. L. Yang, H. A. Padmore, Chemical composition mapping with nanometre resolution by soft x-ray microscopy. *Nat. Photonics* **8**, 765–769 (2014).
34. X. Zhu, A. P. Hitchcock, D. A. Bazylinski, P. Denes, J. Joseph, U. Lins, S. Marchesini, H. W. Shiu, T. Tyliszczak, D. A. Shapiro, Measuring spectroscopy and magnetism of extracted and intracellular magnetosomes using soft x-ray ptychography. *Proc. Natl. Acad. Sci. U.S.A.* **113**, E8219–E8227 (2016).
35. J. Deng, D. J. Vine, S. Chen, Y. S. G. Nashed, Q. Jin, N. W. Phillips, T. Peterka, R. Ross, S. Vogt, C. J. Jacobsen, Simultaneous cryo x-ray ptychographic and fluorescence microscopy of green algae. *Proc. Natl. Acad. Sci. U.S.A.* **112**, 2314–2319 (2015).
36. M. Beckers, T. Senkbeil, T. Gorniak, M. Reese, K. Giewekemeyer, S. C. Gleber, T. Salditt, A. Rosenhahn, Chemical contrast in soft x-ray ptychography. *Phys. Rev. Lett.* **107**, 208101 (2011).
37. A. Tripathi, J. Mohanty, S. H. Dietze, O. G. Shpyrko, E. Shipton, E. E. Fullerton, S. S. Kim, I. McNulty, Dichroic coherent diffractive imaging. *Proc. Natl. Acad. Sci. U.S.A.* **108**, 13393–13398 (2011).
38. O. Kfir, S. Zayko, C. Nolte, M. Sivis, M. Möller, B. Hebler, S. S. P. K. Arekapudi, D. Steil, S. Schäfer, M. Albrecht, O. Cohen, S. Mathias, C. Ropers, Nanoscale magnetic imaging using circularly polarized high-harmonic radiation. *Sci. Adv.* **3**, eaao4641 (2017).
39. H. Jiang, R. Xu, C. C. Chen, W. Yang, J. Fan, X. Tao, C. Song, Y. Kohmura, T. Xiao, Y. Wang, Y. Fei, T. Ishikawa, W. L. Mao, J. Miao, Three-dimensional coherent x-ray diffraction imaging of molten iron in mantle olivine at nanoscale resolution. *Phys. Rev. Lett.* **110**, 205501 (2013).
40. S. Eisebitt, J. Lüning, W. F. Schlotter, M. Lörgen, O. Hellwig, W. Eberhardt, J. Stöhr, Lensless imaging of magnetic nanostructures by x-ray spectro-holography. *Nature* **432**, 885–888 (2004).
41. J. Huijts, S. Fernandez, D. Gauthier, M. Kholodtsova, A. Maghraoui, K. Medjoubi, A. Somogyi, W. Boutu, H. Merdji, Broadband coherent diffractive imaging. *Nat. Photonics* **14**, 618–622 (2020).
42. A. Rana, J. Zhang, M. Pham, A. Yuan, Y. H. Lo, H. Jiang, S. Osher, J. Miao, Potential of attosecond coherent diffractive imaging. *Phys. Rev. Lett.* **125**, 086101 (2019).
43. J. C. H. Spence, U. Weierstall, M. Howells, Phase recovery and lensless imaging by iterative methods in optical, x-ray and electron diffraction. *Philos. Trans. R. Soc. A Math. Phys. Eng. Sci.* **360**, 875–895 (2002).
44. J. W. Goodman, *Introduction to Fourier optics* (Roberts and Company Publishers, ed. 3, 2005).
45. C. S. Williams, O. A. Becklund, *Introduction to the Optical Transfer Function* (SPIE Press, 2002).
46. K. A. Nugent, Coherent methods in the x-ray sciences. *Adv. Phys.* **59**, 1–99 (2010).
47. J. B. Goodenough, The two components of the crystallographic transition in VO_2. *J. Solid State Chem.* **3**, 490–500 (1971).
48. S. Biermann, A. Poteryaev, A. I. Lichtenstein, A. Georges, Dynamical singlets and correlation-assisted peierls transition in VO_2. *Phys. Rev. Lett.* **94**, 026404 (2005).
49. T. C. Koethe, Z. Hu, M. W. Haverkort, C. Schüßler-Langeheine, F. Venturini, N. B. Brookes, O. Tjernberg, W. Reichelt, H. H. Hsieh, H. J. Lin, C. T. Chen, L. H. Tjeng, Transfer of spectral weight and symmetry across the metal-insulator transition in VO_2. *Phys. Rev. Lett.* **97**, 116402 (2006).
50. A. Gloter, V. Serin, C. Turquat, C. Cesari, C. Leroux, G. Nihoul, Vanadium valency and hybridization in V-doped hafnia investigated by electron energy loss spectroscopy. *Eur. Phys. J. B.* **22**, 179–186 (2001).
51. N. B. Aetukuri, A. X. Gray, M. Drouard, M. Cossale, L. Gao, A. H. Reid, R. Kukreja, H. Ohldag, C. A. Jenkins, E. Arenholz, K. P. Roche, H. A. Dürr, M. G. Samant, S. S. P. Parkin, Control of the metal-insulator transition in vanadium dioxide by modifying orbital occupancy. *Nat. Phys.* **9**, 661–666 (2013).
52. E. Goering, O. Müller, M. Klemm, M. L. DenBoer, S. Horn, Angle dependent soft-x-ray absorption spectroscopy of V_2O_5. *Philos. Mag. B* **75**, 229–236 (1997).
53. J. Y. Suh, R. Lopez, L. C. Feldman, R. F. Haglund, Semiconductor to metal phase transition in the nucleation and growth of VO_2 nanoparticles and thin films. *J. Appl. Phys.* **96**, 1209–1213 (2004).
54. R. E. Marvel, R. R. Harl, V. Craciun, B. R. Rogers, R. F. Haglund Jr., Influence of deposition process and substrate on the phase transition of vanadium dioxide thin films. *Acta Mater.* **91**, 217–226 (2015).
55. L. Vidas, C. M. Günther, T. A. Miller, B. Pfau, D. Perez-Salinas, E. Martínez, M. Schneider, E. Gührs, P. Gargiani, M. Valvidares, R. E. Marvel, K. A. Hallman, R. F. Haglund, S. Eisebitt, S. Wall, Imaging nanometer phase coexistence at defects during the insulator–metal phase transformation in VO_2 thin films by resonant soft x-ray holography. *Nano Lett.* **18**, 3449–3453 (2018).
56. J. H. Park, J. M. Coy, T. Serkan Kasirga, C. Huang, Z. Fei, S. Hunter, D. H. Cobden, Measurement of a solid-state triple point at the metal–insulator transition in VO_2. *Nature* **500**, 431–434 (2013).
57. M. G. Brik, K. Ogasawara, H. Ikeno, I. Tanaka, Fully relativistic calculations of the $L_{2,3}$-edge XANES spectra for vanadium oxides. *Eur. Phys. J. B.* **51**, 345–355 (2006).
58. P. Guttmann, C. Bittencourt, S. Rehbein, P. Umek, X. Ke, G. Van Tendeloo, C. P. Ewels, G. Schneider, Nanoscale spectroscopy with polarized x-rays by NEXAFS-TXM. *Nat. Photonics* **6**, 25–29 (2012).
59. S. Flewett, C. M. Günther, C. v. K. Schmising, B. Pfau, J. Mohanty, F. Büttner, M. Riemeier, M. Hantschmann, M. Kläui, S. Eisebitt, Holographically aided iterative phase retrieval. *Opt. Express* **20**, 29210–29216 (2012).
60. F. Büttner, B. Pfau, M. Böttcher, M. Schneider, G. Mercurio, C. M. Günther, P. Hessing, C. Klose, A. Wittmann, K. Gerlinger, L. M. Kern, C. Strüber, C. von Korff Schmising, J. Fuchs, D. Engel, A. Churikova, S. Huang, D. Suzuki, I. Lemesh, M. Huang, L. Caretta, D. Weder, J. H. Gaida, M. Möller, T. R. Harvey, S. Zayko, K. Bagschik, R. Carley, L. Mercadier, J. Schlappa, A. Yaroslavtsev, L. Le Guyarder, N. Gerasimova, A. Scherz, C. Deiter, R. Gort, D. Hickin, J. Zhu, M. Turcato, D. Lomidze, F. Erdinger, A. Castoldi, S. Maffessanti, M. Porro, A. Samartsev, J. Sinova, C. Ropers, J. H. Mentink, B. Dupé, G. S. D. Beach, S. Eisebitt, Observation of fluctuation-mediated picosecond nucleation of a topological phase. *Nat. Mater.* **20**, 30–37 (2021).
61. A. S. Johnson, D. R. Austin, D. A. Wood, C. Brahms, A. Gregory, K. B. Holzner, S. Jarosch, E. W. Larsen, S. Parker, C. S. Strüber, P. Ye, J. W. G. Tisch, J. P. Marangos, High-flux soft x-ray harmonic generation from ionization-shaped few-cycle laser pulses. *Sci. Adv.* **4**, eaar3761 (2018).
62. M. F. Jager, C. Ott, P. M. Kraus, C. J. Kaplan, W. Pouse, R. E. Marvel, R. F. Haglund, D. M. Neumark, S. R. Leone, Tracking the insulator-to-metal phase transition in VO_2 with few-femtosecond extreme UV transient absorption spectroscopy. *Proc. Natl. Acad. Sci. U.S.A.* **114**, 9558–9563 (2017).
63. A. Pattammattel, R. Tappero, M. Ge, Y. S. Chu, X. Huang, Y. Gao, H. Yan, High-sensitivity nanoscale chemical imaging with hard x-ray Nano-XANES. *Sci. Adv.* **6**, eabb3615 (2020).
64. D. H. Parks, X. Shi, S. D. Kevan, Partially coherent x-ray diffractive imaging of complex objects. *Phys. Rev. A* **89**, 063824 (2014).
65. L. W. Whitehead, G. J. Williams, H. M. Quiney, D. J. Vine, R. A. Dilanian, S. Flewett, K. A. Nugent, A. G. Peele, E. Balaur, I. McNulty, Diffractive imaging using partially coherent x rays. *Phys. Rev. Lett.* **103**, 243902 (2009).
66. J. N. Clark, X. Huang, R. Harder, I. K. Robinson, High-resolution three-dimensional partially coherent diffraction imaging. *Nat. Commun.* **3**, 993–996 (2012).
67. J. R. Fienup, Reconstruction of an object from the modulus of its Fourier transform. *Opt. Lett.* **3**, 27–29 (1978).
68. L. B. Lucy, An iterative technique for the rectification of observed distributions. *Astron. J.* **79**, 745 (1974).
69. W. H. Richardson, Bayesian-based iterative method of image restoration*. *J. Opt. Soc. Am.* **62**, 55 (1972).

Acknowledgments

Funding: This project has received funding from the European Research Council (ERC) under the European Union's Horizon 2020 Research and Innovation Programme (grant agreement no. 758461) and under the Marie Skłodowska-Curie grant agreement no. 754510 (PROBIST) as well as the Ministry of Science, Innovation and Universities (MCIU), State Research Agency (AEI), and European Regional Development Fund (FEDER) PGC2018-097027-B-I00 and was supported by Spanish MINECO (Severo Ochoa grants SEV-2015-0522 and SEV2015-0496) as well as Fundació Privada Cellex and CERCA Programme/Generalitat de Catalunya. L.V. acknowledges financial support by the HZB. Research at Vanderbilt was supported by the NSF EECS-1509740. **Author contributions:** S.E. and S.W. conceived the project. K.A.H. and R.F.H. grew the samples, which were processed by C.M.G. subsequently. L.V., D.P.-S., C.M.G., and B.P. measured the diffraction patterns. A.S.J., J.V.C., and D.P.-S. processed the images, and A.S.J. analyzed the data. A.S.J. and S.W. wrote the manuscript with input from all authors. **Competing interests:** The authors declare that they have no competing interests. **Data and materials availability:** All data needed to evaluate the conclusions in the paper are present in the paper and/or the Supplementary Materials. Additional data related to this paper may be requested from the authors.

Submitted 11 January 2021
Accepted 22 June 2021
Published 11 August 2021
10.1126/sciadv.abf1386

Citation: A. S. Johnson, J. V. Conesa, L. Vidas, D. Perez-Salinas, C. M. Günther, B. Pfau, K. A. Hallman, R. F. Haglund Jr., S. Eisebitt, S. Wall, Quantitative hyperspectral coherent diffractive imaging spectroscopy of a solid-state phase transition in vanadium dioxide. *Sci. Adv.* **7**, eabf1386 (2021).

ScienceAdvances

Quantitative hyperspectral coherent diffractive imaging spectroscopy of a solid-state phase transition in vanadium dioxide

Allan S. JohnsonJordi Valls ConesaLuciana VidasDaniel Perez-SalinasChristian M. GüntherBastian PfauKent A. HallmanRichard F. Haglund Jr.Stefan EisebittSimon Wall

Sci. Adv., 7 (33), eabf1386. • DOI: 10.1126/sciadv.abf1386